OPEN ACCESS
Journal of Innovative Optical Health Sciences
Vol. 14, No. 2 (2021) 2041006 (8 pages)

DOI: 10.1142/S1793545820410060

World Scientific
www.worldscientific.com

Observations of intracellular second-harmonic generation imaging in black phosphorus nanosheets

Xiao Peng, Yiwan Song, Zheng Peng, Kaixuan Nie,
Hao Liu, Yingxin Zhou, Feifan Zhou, Yufeng Yuan*,‡,
Jun Song†,‡ and Junle Qu
Center for Biomedical Optics and Photonics (CBOP) &
College of Physics and Optoelectronic Engineering
Key Laboratory of Optoelectronic Devices and Systems of
Ministry of Education and Guangdong Province
Shenzhen University, Shenzhen 518060, P. R. China
**yfyuan@szu.edu.cn*
†*songjun@szu.edu.cn*

Received 11 August 2020
Accepted 20 September 2020
Published 21 October 2020

Functionalized black phosphorus (BP) nanosheets have been considered as promising nanoagents in cancer therapy due to their excellent photothermal conversion efficiency. However, it is still difficult to visually monitor the dynamic localization of BP nanoagents in cancer cells. In this paper, we systematically studied the second-harmonic generation (SHG) signals originating from exfoliated BP nanosheets. Interestingly, under the excitation of a high frequency pulsed laser at 950 nm, the SHG signals of BP nanosheets *in vitro* are almost undetectable because of their poor stability. However, the intracellular SHG signals from BP nanosheets could be measured by *in vivo* optical imaging due to the efficient enrichment of living HeLa cells. Moreover, the SHG signal intensity from BP nanosheets increases with the prolonged incubation time. It can be expected that the BP nanosheets could be a promising intracellular SHG nanoprobe employed for visually *in vivo* biomedical imaging in practical cancer photothermal therapy (PIT).

Keywords: Second harmonic generation nanoprobe; black phosphorus nanosheets; *in vivo* imaging; HeLa cells; visual monitoring.

1. Introduction

Biomedical optical imaging has been an essential approach in cancer diagnosis and therapy. Owing to their intriguing features such as noninvasiveness, deep penetration depth, high sensitivity, and high resolution, nonlinear optical techniques including two-photon excitation fluorescence (TPEF) and second-harmonic generation (SHG) have been

‡Corresponding authors.

successfully employed in *in vivo* biomedical optical imaging.[1,2] Typically, the second-harmonic signal with a 2ω frequency can be generated when an optical wave with a ω frequency penetrates through a noncentrosymmetric microstructure.[3] Generally, the excitation of optical wave is a pulsed laser because the power of pulsed light is enough for the generation of anharmonic signals.[4] Prior to the SHG measurement, any staining or pretreatment for samples is no longer needed. In addition, unlike fluorescent signals suffering from significant limitations such as saturation, bleaching, and blinking, the SHG signals do not saturate with the increasing intensity of excitation light. In view of these advantages, it is of considerable significance to design novel SHG nanoprobe for *in vivo* biomedical imaging.

Most recently, there is an increasing attention in studying two-dimensional (2D) materials-based nonlinear optical properties. It has been demonstrated that few layered 2D materials such as graphene,[5–7] hexagonal boron nitride,[8,9] transition metal dichalcogenides (TMDCs),[8,10–12] have shown strong second-order nonlinear optical response due to the quantum confinement in noncentrosymmetric crystal structures. Very recently, Huang *et al.*[13] demonstrated a highly stable harmonic pulse generation using the nonlinear saturated absorption feature originating from 2D material MXene (V_2CT_x). Unlike other 2D material crystals with planar honeycomb structure, the new superstar black phosphorus (BP) has a puckered honeycomb lattice, resulting in significant in-plane anisotropy.[14–16] It is worth noting that the large anisotropy of BP can produce novel physical phenomena such as nonlinear saturable absorption and optical Kerr effect.[17] To date, the studies on nonlinear optical effect of BP are still in their nascent stage. Theoretically, Hipolito *et al.*[18] reported a calculation of third harmonic generation (THG) in BP. In addition, Zhou *et al.*[19] theoretically investigated the second harmonic wave in BP nanoflakes using finite difference time-domain method. Experimentally, Wu *et al.*[20] observed that the THG response from multilayer BP flakes is highly dependent on the polarization of excitation light due to its significant anisotropy. Also, Rodrigues *et al.*[21] reported the nonlinear THG in few-layered BP, showing that the THG signals is three orders of magnitude larger than that of graphene. In addition, Youngblood *et al.*[22] observed the layer-tunable THG at 519 nm in multilayer BP using an ultrafast near-IR laser at 1557 nm. Afterwards, Autere *et al.*[23] characterized the THG from exfoliated BP nanosheets employing a scanning multi-photon microscopy. It is worth noting that those observations mainly focus on the basic nonlinear optical responses of BP *in vitro*. Up to now, there is no report on the nonlinear optical response from BP in living cells or tissues.

To date, photothermal therapy (PIT) has been a promising strategy employed for cancer nanomedicine.[24] In particular, engineered BP nanostructures also have shown great potential in PIT because of good photothermal conversion efficiency.[25–27] Recently, various engineered BP and BP analogs have been successfully employed in PIT applications[28–33] due to their excellent biocompatibility and biodecomposability. However, it is an important but still a difficult task to visually trace the dynamic localization of black phosphorus nanoagents during the cancer therapy. The precise orientation of BP nanoagents in cancer cells can significantly improve photothermal treatment effects. Herein, we first reported the observation in localization of BP nanosheets using SHG imaging technique in HeLa cells. Few-layered BP nanosheets were fabricated by a liquid-phase exfoliation approach. Under the illumination of a pulsed laser at 950 nm, the obvious SHG signals from BP nanosheets treated with HeLa cells can be obtained by *in vivo* imaging, due to the possibly existing intracellular enrichment effect. We believe that the intriguing SHG feature originating from BP nanosheets has promising application in real-time monitoring the dynamic localization of BP nanoagents in practical cancer therapy.

2. Materials and Methods

2.1. *Materials*

BP crystal (99.998%) stored in a sealed glass tube was obtained from Nanjing XFNANO Materials Tech Co., Ltd. Rhodamine 6G was purchased from Beyotime Biotechnology. Cell Counting Kit-8 (CCK8) assay kits were purchased from KeyGen BioTech. N-Methyl pyrrolidone (NMP, 99%, ReagentPlus) was purchased from Sigma-Aldrich. Ethanol (100%) was bought from Aladdin Reagents. HeLa cells were obtained from American Type Culture Collection, USA. The reagents employed for cell culture (such as Dulbecco minimum essential medium (DMEM), penicillin-streptomycin, and fetal bovine serum) were purchased from Hyclone. All the

chemical reagents were used without further purification. The ultrapure water with a resistivity of 18.2 MΩ/cm was used in all the experiments.

2.2. *Liquid-phase exfoliation of BP nanosheets and characterization*

Under an ice bath, the BP nanosheets in the NMP were exfoliated from BP bulk counterpart using an ultrasound sonication technique. According to the previously reported method with some modifications,[34] 60 mg BP powder was added into a 100 mL sealed beaker containing 50 mL NMP. Under an operation power of 800 mW, the solvent NMP containing BP powder was continuously sonicated for 8 h by a sonic tip. The working time of ultrasound probe is 2 s, and there is a 4 s interval before the next work time. To remove large size BP nanosheets, the obtained mixture was centrifuged for 20 min at 5000 rpm. Then, the supernatant was further centrifuged for 20 min at 10,000 rpm. Finally, the obtained precipitate was washed twice by ethanol and ultrapure water, respectively. The obtained BP nanosheets were re-suspended in ultrapure water. The characterization of BP nanosheets was performed on a transmission electron microscope (JEM-1230 CX, JEOL Ltd, Japan) with an operation voltage at 200 kV. The absorption spectra of BP nanosheets in ultrapure water were obtained with a UV-Vis spectrophotometer (UV 1780, Shimadzu, Japan). The Raman scattering of BP nanosheets and bulk BP crystal was recorded using a high-resolution confocal Raman spectrometer (Renishaw, inVia) equipped with a 785 nm laser as the excitation wavelength.

2.3. *Cell culture and cytotoxicity assay*

Under a condition of 5% carbon dioxide (CO_2) and humidity, HeLa cells were placed in a temperature-controlled incubator at 37°C, and continuously cultured in DMEM containing 10% fetal bovine serum, and 1% penicillin-streptomycin.

In order to evaluate the biocompatibility of obtained BP nanosheets, a standard cytotoxicity assay by using CCK-8 kit was performed onto HeLa cells.[35] In 96-well plates, approximately 10,000 of HeLa cells were seeded into each well and further cultured overnight for attachment. The next day, various concentrations of BP nanosheets (25, 50, 100, and 200 μg/mL) were added onto the HeLa cells. For each concentration, there were six replicates. After incubation for 24 h, the solution in each well was extracted. Then, the mixture solutions containing 10 μL CCK-8 and 100 μL fresh culture medium were added into each well. After another incubation time for around 1–2 h, the chromogenic reaction occurred. For each well, the OD value at 450 nm wavelength was measured using a microplate reader.

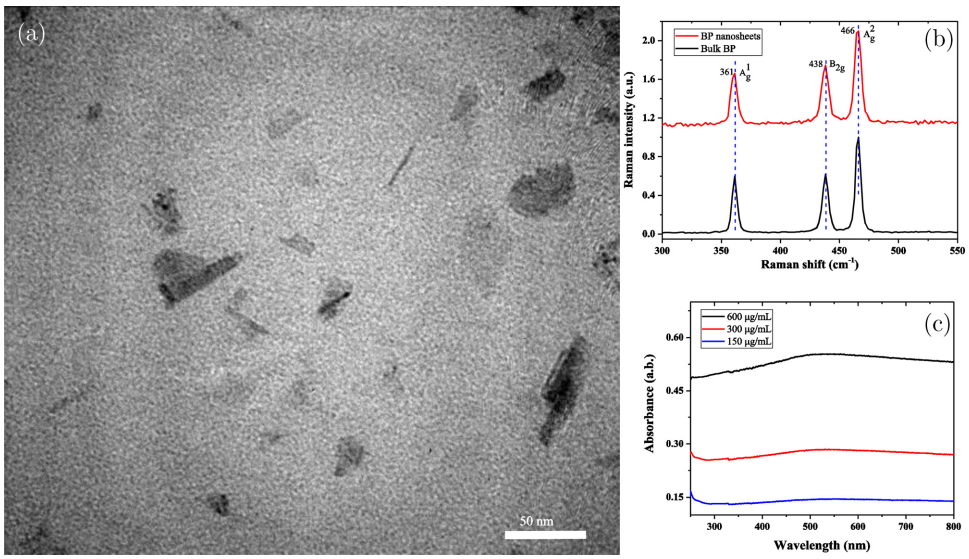

Fig. 1. (a) TEM image of BP nanosheets. Scale bar: 50 nm. (b) Raman spectra of BP nanosheets (red) and bulk BP crystal (black). (c) Absorbance spectra of the BP nanosheets in ultrapure water at different concentrations (600 μg/mL (black), 300 μg/mL (red), 150 μg/mL (blue)).

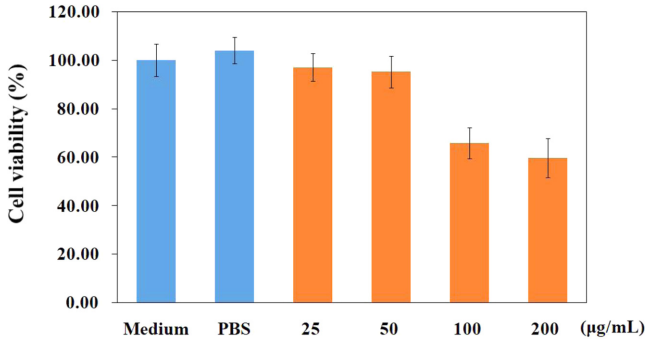

Fig. 2. Cell viability of Hela cells after 24 h incubation with cell culture, PBS buffer solution, and different concentrations of BP nanosheets (25, 50, 100, and 200 μg/mL).

2.4. *SHG imaging*

Prior to SHG imaging, HeLa cells were stained with Rhodamine 6G solutions. After 1 h incubation, the cell lines were washed thrice using PBS buffer solution. Next, the cell lines were uniformly seeded into four cell confocal dishes. For every 2 h, 50 μL 500 μg/mL BP nanosheets were added into the cell lines, respectively. After 6 h, the four samples were washed twice by PBS buffer solution, respectively. All the transmission and SHG images were obtained by a Leica super-resolution microsystem (TCS SP8 STED 3X).[36,37] All the images were measured at the focal plane of the 100× oil objective with high N.A of 1.4. To excite the SHG signals, a pulsed laser (Spectra-Physics) with 80 MHz pulse rate was used. The SHG imaging of BP nanosheets *in vitro* and *in vivo* was measured. In this experiment, we first selected 850, 900, 950, 1000, and 1100 nm as the excitation wavelength to generate the SHG signals. The corresponding detection interval of SHG signals is 415–435 nm, 440–460 nm, 465–485 nm, 490–510 nm, and 540–560 nm, respectively. In addition, the fluorescence of Rhodamine 6G was measured by single photon excitation of 514 nm.

3. Results and Discussion

The BP nanosheets were exfoliated from bulk BP crystal, and eventually suspended in ultrapure water. Transmission electron microscopy (TEM) was used to examine the morphology of exfoliated BP nanosheets, as shown in Fig. 1(a). A general profile of the BP nanosheets demonstrated that the lateral sizes of BP nanosheets range from 30 to 60 nm. Therefore, the sizes of obtained BP nanosheets make it possible for entering living cells through efficient cell endocytosis. In addition, the BP nanosheets were characterized by Raman spectroscopy, as shown in Fig. 1(b). There are three strong Raman bands located at 361 cm^{-1} (A_g^1: out-of-plane phonon mode), 438 cm^{-1} (B_{2g}: in-plane phonon mode), and 466 cm^{-1} (A_g^2: in-plane phonon mode), respectively. Figure 1(c) shows that there is

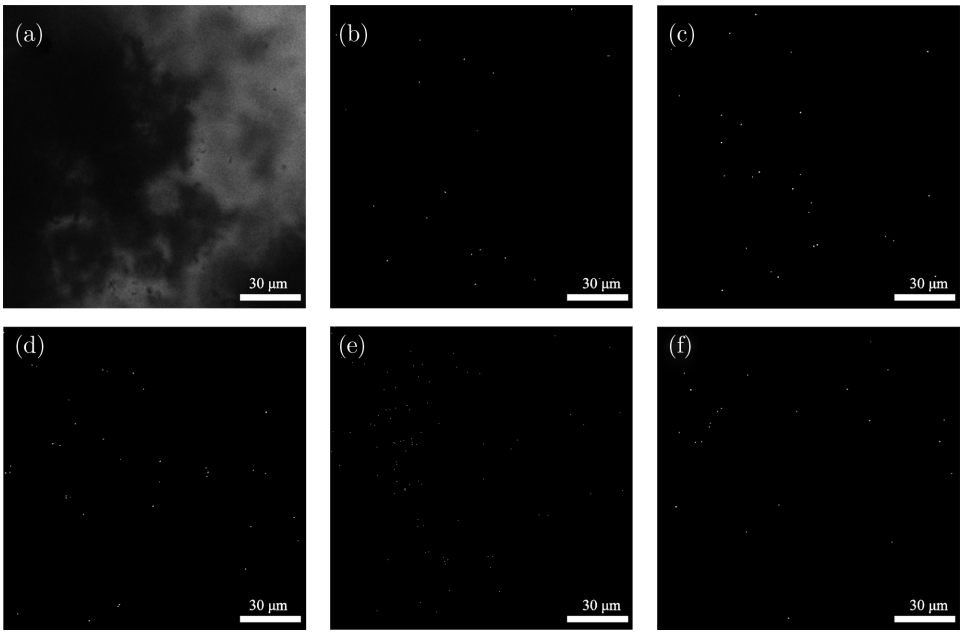

Fig. 3. (a) Transmission image of BP nanosheets *in vitro*; The SHG images of BP nanosheets excited by the wavelength at 850 nm (b), 900 nm (c), 950 nm (d), 1000 nm (e), and 1100 nm (f), respectively.

a broad absorption behavior from 400 nm to 800 nm, indicating the BP nanoparticles can be employed to perform PIT.

Prior to performing the intracellular nonlinear optical effects, the BP nanosheets employed for the following endocytosis should have good biocompatibility. Therefore, we studied the relative cell viabilities of HeLa cells after 24 h incubation with BP nanosheets at a series of concentrations such as 20, 50, 100, and 200 μg/mL, as shown in Fig. 2. To better compare the cell cytotoxicity assay, the control samples that HeLa cells incubated with medium and PBS were also introduced. The obtained results show that, after 24 h incubation, the higher the BP nanosheets concentration, the worse the cell viability. However, when the concentration of BP nanosheets reaches up to 200 μg/mL, HeLa cells still have high viability (more than 50%), indicating that the exfoliated BP nanosheets is suitable for performing the intracellular bioimaging.

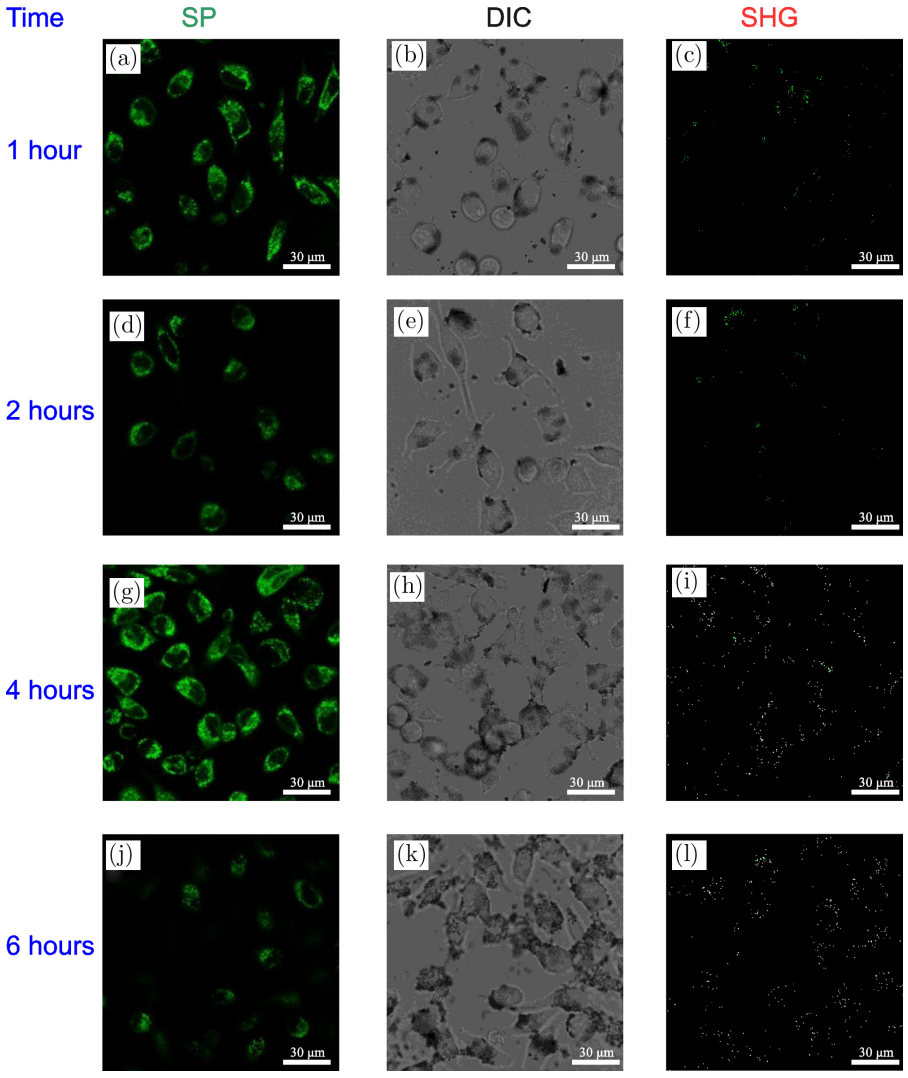

Fig. 4. The single photon excitation fluorescence images of HeLa cells treated with Rhodamine 6G *with respect to* different incubation time such as 1 h, (a) 2 h, (d) 4 h, (g) and 6 h (j). The differential interference contrast images of HeLa cells treated with BP nanosheets *with respect to* different incubation time such as 1 h (b) 2 h, (e) 4 h, (h) and 6 h (k). The SHG images of BP nanosheets in HeLa cells *with respect to* different incubation time such as 1 h, (c) 2 h, (f) 4 h, (i) and 6 h. (l) *Note*: SP stands for single photon; DIC denotes differential interference contrast; SHG corresponds to SHG. For Rhodamine 6G signals, the excitation wavelength was 514 nm, the emission range is 525–625 nm. For SHG signals, the excitation wavelength was 950 nm, and the emission range is 465–485 nm.

It is worth mentioning that the near infrared (NIR) window is indispensable to perform deep nonlinear optical imaging including TPEF and SHG, because it can avoid strong autofluorescence. Generally, both the NIR-I window from 700–950 nm and NIR-II window ranging from 1000–1700 nm are widely used.[38] In this study, the SHG signals of BP nanosheets *in vitro* were investigated by a supercontinuum white laser with 80 MHz pulse rate, as shown in Fig. 3. Unfortunately, there is no detectable signal from the BP nanosheets by varying various excitation wavelengths such as 850, 900, 950, 1000, and 1100 nm. The possible reason is that the BP nanosheets exposed to a high-power pulsed laser are unstable, and the BP nanosheets could be broken into small pieces, due to the continuous illumination of a pulsed laser.

However, after the BP nanosheets were incubated with live HeLa cells, the significant SHG signals of BP nanosheets can be obtained by *in vivo* imaging, as shown in Fig. 4. To illustrate the position of BP nanosheets in HeLa cells, both the single photon fluorescence and differential interference contrast images originating from HeLa cells stained with Rhodamine 6G were carried out. The detected fluorescence signals in Figs. 4(a), 4(d), 4(g), and 4(j), originated from Rhodamine 6G molecules. In addition, no SHG signals could be detected from the HeLa cells. With the help of cell incubation, the BP nanosheets can enter Hela cells. The four images including Figs. 4(c), 4(f), 4(i), and 4(l) clearly demonstrate that the obtained SHG signals in Hela cells are from the BP nanosheets. Moreover, as the incubation time is prolonged, the SHG intensity becomes stronger. It can be found that the SHG signals of BP nanosheets in HeLa cells are distinct from *in vitro* measurement. A possible reason is that the HeLa cells can efficiently accumulate the BP nanosheets, forming some hot spots with relative high concentrations. It is worth noting that compared to other 2D TMDCs such as MoS_2 nanosheets with strong photoluminescence,[39,40] BP nanosheets almost have no photon luminescence. So, there is no signal interference from two photon excitation fluorescence during SHG imaging. In addition, due to the strong interactions between MoS_2 nanosheets and Hella cells, the MoS_2 nanosheets usually suffer from fluorescence quenching. However, there is no quenching for BP nanosheets. Therefore, our observations have shown the feasibility that BP nanosheets can act as an excellent SHG nanoprobe for *in vivo* bioimaging.

4. Conclusions

In this study, we reported the discovery that BP nanosheets can produce detectable SHG signals in HeLa cells. Under the excitation of a high-frequency pulsed laser at 950 nm, the SHG signals of BP nanosheets *in vitro* is almost undetectable, due to their poor stability. However, the intracellular SHG signals from BP nanosheets can be detected by *in vivo* bioimaging, after the BP nanosheets were treated with HeLa cells. Furthermore, the intensity of SHG signals from BP nanosheets in HeLa cells increases with the prolongation of incubation time, due to the possibly existing intracellular enrichment effect. In view of the interesting nonlinear second-order feature, the BP nanosheets could work as a potential SHG nanoprobe for visually *in vivo* optical imaging during cancer therapy.

Conflicts of Interest

The authors declare no competing professional and financial interest.

Acknowledgments

This work has been partially supported by the National Key R&D Program of China (2018YFC0910602), the National Natural Science Foundation of China (31771584/62075137/61775145/61525503/61620106016/61835009), Project of Department of Education of Guangdong Province (2016KCXTD007), Guangdong Basic and Applied Basic Research Foundation (2020A1515010377), Guangdong Province Key Area R&D Program (2019B110233004), Shenzhen Basic Research Project (JCYJ20170818100153423), and Science Foundation of Shenzhen University (Grant No. 2017000193).

References

1. H. Li, J. Yu, R. Zhang *et al.*, "Two-photon excitation fluorescence lifetime imaging microscopy: A promising diagnostic tool for digestive tract tumors," *J. Innov. Opt. Heal. Sci.* **12**, 1930009 (2019).
2. C. Li, R. K. Pastila, C. P. Lin, "Label-free imaging immune cells and collagen in atherosclerosis with

two-photon and second harmonic generation microscopy," *J. Innov. Opt. Heal. Sci.* **9**, 1640003 (2015).
3. Y. R. Shen, "Surface properties probed by second-harmonic and sum-frequency generation," *Nature* **337**, 519–525 (1989).
4. Y. Wang, J. Xiao, S. Yang *et al.*, "Second harmonic generation spectroscopy on two-dimensional materials [Invited]," *Opt. Mater. Exp.* **9**, 1136–1149 (2019).
5. J. J. Dean, H. M. van Driel, "Graphene and few-layer graphite probed by second-harmonic generation: Theory and experiment," *Phys. Rev. B* **82**, 125411 (2010).
6. Y. W. Shan, Y. G. Li, D. Huang *et al.*, "Stacking symmetry governed second-harmonic generation in graphene trilayers," *Sci. Adv.* **4**, eaat0074 (2018).
7. Y. Zhang, D. Huang, Y. W. Shan *et al.*, "Doping-induced second-harmonic generation in centrosymmetric graphene from quadrupole response," *Phys. Rev. Lett.* **122**, 047401 (2019).
8. Y. L. Li, Y. Rao, K. F. Mak *et al.*, "Probing symmetry properties of few-layer MoS2 and h-BN by optical second-harmonic generation," *Nano Lett.* **13**, 3329–3333 (2013).
9. S. Kim, J. E. Froch, A. Gardner *et al.*, "Second-harmonic generation in multilayer hexagonal boron nitride flakes," *Opt. Lett.* **44**, 5792–5795 (2019).
10. X. B. Yin, Z. L. Ye, D. A. Chenet *et al.*, "Edge nonlinear optics on a MoS_2 atomic monolayer," *Science* **344**, 488–490 (2014).
11. G. Wang, X. Marie, I. Gerber *et al.*, "Giant enhancement of the optical second-harmonic emission of WSe2 monolayers by laser excitation at exciton resonances," *Phys. Rev. Lett.* **114**, 097403 (2015).
12. K. L. Seyler, J. R. Schaibley, P. Gong *et al.*, "Electrical control of second-harmonic generation in a WSe2 monolayer transistor," *Nat. Nanotech.* **10**, 407–411 (2015).
13. H. Weichun, M. Chunyang, L. Chao *et al.*, "Highly stable MXene (V2CTx)-based harmonic pulse generation," *Nanophoton.* **9**, 2577–2585 (2020).
14. W. Y. Lei, G. Liu, J. Zhang *et al.*, "Black phosphorus nanostructures: Recent advances in hybridization, doping and functionalization," *Chem. Soc. Rev.* **46**, 3492–3509 (2017).
15. J. L. Zhao, J. J. Zhu, R. Cao *et al.*, "Liquefaction of water on the surface of anisotropic two-dimensional atomic layered black phosphorus," *Nat. Commun.* **10**, 4062 (2019).
16. Y. F. Yuan, X. T. Yu, Q. L. Ouyang *et al.*, "Highly anisotropic black phosphorous-graphene hybrid architecture for ultrassensitive plasmonic biosensing: Theoretical insight," *2D Mater.* **5**, 025015 (2018).
17. X. Chen, J. S. Ponraj, D. Y. Fan *et al.*, "An overview of the optical properties and applications of black phosphorus," *Nanoscale* **12**, 3513–3534 (2020).
18. F. Hipolito, T. G. Pedersen, "Optical third harmonic generation in black phosphorus," *Phys. Rev. B* **97**, 035431 (2018).
19. R. L. Zhou, J. Peng, S. Yang *et al.*, "Lifetime and nonlinearity of modulated surface plasmon for black phosphorus sensing application," *Nanoscale* **10**, 18878–18891 (2018).
20. H.-Y. Wu, Y. Yen, C.-H. Liu, "Observation of polarization and thickness dependent third-harmonic generation in multilayer black phosphorus," *Appl. Phys. Lett.* **109**, 261902 (2016).
21. M. J. L. F. Rodrigues, C. J. S. de Matos, Y. W. Ho *et al.*, "Resonantly increased optical frequency conversion in atomically thin black phosphorus," *Adv. Mater.* **28**, 10693–10700 (2016).
22. N. Youngblood, R. Peng, A. Nemilentsau *et al.*, "Layer-tunable third-harmonic generation in multilayer black phosphorus," *ACS Photon.* **4**, 8–14 (2017).
23. A. Autere, C. R. Ryder, A. Säynätjoki *et al.*, "Rapid and large-area characterization of exfoliated black phosphorus using third-harmonic generation microscopy," *J. Phys. Chem. Lett.* **8**, 1343–1350 (2017).
24. Z. Xie, T. Fan, J. An *et al.*, "Emerging combination strategies with phototherapy in cancer nanomedicine," *Chem. Soc. Rev.* doi: 10.1039/D0CS00215A (2020).
25. S. Xiong, X. Chen, Y. Liu *et al.*, "Black phosphorus as a versatile nanoplatform: From unique properties to biomedical applications," *J. Innov. Opt. Heal. Sci.* **13**, 2030008 (2020).
26. J. D. Shao, H. H. Xie, H. Huang *et al.*, "Biodegradable black phosphorus-based nanospheres for in vivo photothermal cancer therapy," *Nat. Commun.* **7**, 12967 (2016).
27. M. Qiu, D. Wang, W. Y. Liang *et al.*, "Novel concept of the smart NIR-light-controlled drug release of black phosphorus nanostructure for cancer therapy," *Proc. Natl. Acad. Sci. USA* **115**, 501–506 (2018).
28. C. Xing, S. Chen, M. Qiu *et al.*, "Conceptually novel black phosphorus/cellulose hydrogels as promising photothermal agents for effective cancer therapy," *Nat. Commun.* **7**, 1701510 (2018).
29. X. Liang, X. Ye, C. Wang *et al.*, "Photothermal cancer immunotherapy by erythrocyte membrane-coated black phosphorus formulation," *J. Control. Release* **296**, 150–161 (2019).
30. D. An, J. Fu, Z. Xie *et al.*, "Progress in the therapeutic applications of polymer-decorated black phosphorus and black phosphorus analog nanomaterials in biomedicine," *J. Mater. Chem. B* **8**, 7076–7120 (2020).

31. H. Hu, Z. Shi, K. Khan *et al.*, "Recent advances in doping engineering of black phosphorus," *J. Mater. Chem. A* **8**, 5421–5441 (2020).
32. M. Qiu, A. Singh, D. Wang *et al.*, "Biocompatible and biodegradable inorganic nanostructures for nanomedicine: Silicon and black phosphorus," *Nano Today* **25**, 135–155 (2019).
33. M. Qiu, W. X. Ren, T. Jeong *et al.*, "Omnipotent phosphorene: A next-generation, two-dimensional nanoplatform for multidisciplinary biomedical applications," *Chem. Soc. Rev.* **47**, 5588–5601 (2018).
34. Z. B. Sun, H. H. Xie, S. Y. Tang *et al.*, "Ultrasmall black phosphorus quantum dots: Synthesis and use as photothermal agents," *Angew. Chem. Int. Edn.* **54**, 11526–11530 (2015).
35. H. Liang, Z. Peng, X. Peng *et al.*, "Fluorescence lifetime imaging microscopy (FLIM) monitors tumor cell death triggered by photothermal therapy with MoS_2 nanosheets," *J. Innov. Opt. Heal. Sci.* **12**, 1940002 (2019).
36. L. L. Liang, W. Yan, X. Qin *et al.*, "Designing sub-2 nm organosilica nanohybrids for far-field super-resolution imaging," *Angew. Chem. Int. Edn.* **59**, 746–751 (2020).
37. H. Li, S. Ye, J. Q. Guo *et al.*, "Biocompatible carbon dots with low-saturation-intensity and high-photobleaching-resistance for STED nanoscopy imaging of the nucleolus and tunneling nanotubes in living cells," *Nano Res.* **12**, 3075–3084 (2019).
38. J. Zhao, D. Zhong, S. Zhou, "NIR-I-to-NIR-II fluorescent nanomaterials for biomedical imaging and cancer therapy," *J. Mater. Chem. B* **6**, 349–365 (2018).
39. A. Splendiani, L. Sun, Y. Zhang *et al.*, "Emerging photoluminescence in monolayer MoS2," *Nano Lett.* **10**, 1271–1275 (2010).
40. A. Granados del Águila, S. Liu, T. T. H. Do *et al.*, "Linearly polarized luminescence of atomically thin MoS2 semiconductor nanocrystals," *ACS Nano* **13**, 13006–13014 (2019).